A numerical study of the high-*n* shear Alfvén spectrum gap and the high-*n* gap mode

Cite as: Physics of Fluids B: Plasma Physics **4**, 3713 (1992); https://doi.org/10.1063/1.860327
Submitted: 18 May 1992 . Accepted: 23 July 1992 . Published Online: 04 June 1998

M. S. Chu, J. M. Greene, L. L. Lao, A. D. Turnbull, and M. S. Chance

A numerical study of the high-n shear Alfvén spectrum gap and the high-n gap mode

M. S. Chu, J. M. Greene, L. L. Lao, A. D. Turnbull, and M. S. Chance[a)]
General Atomics, San Diego, California 92186-9784

(Received 18 May 1992; accepted 23 July 1992)

The toroidicity-induced gaps of the shear Alfvén wave spectrum in tokamaks are shown to satisfy an envelope equation. The structure of these gaps, and the location of the high-n gap modes, which are localized modes with frequency in the gap, are studied for general numerically generated equilibria. The dependence of the frequencies of the gaps and the gap modes on the equilibrium properties, such as elongation, triangularity, and β of the plasma are explored.

I. INTRODUCTION

The toroidicity-induced Alfvén eigenmode (TAE mode) has been predicted to be unstable in a fusion plasma.[1] These modes are destabilized by alpha particles through the inverse Landau damping process. In present-day experiments, these modes have been observed both in the Tokamak Fusion Test Reactor[2] (TFTR) and DIII-D,[3] where they are destabilized by the energetic particles created by the charge exchange ionization of the neutral beam.

The frequency of the TAE mode is given by $\omega \sim v_A/2qR$. Since its energy comes from the expansion energy of the hot particles, the diamagnetic frequency of the hot particles has to satisfy the criterion of $\omega_h^*/\omega > 1$.[1,4] Since $\omega_h^* \propto n$, n being the toroidal mode number, this criterion favors the excitation of higher n modes. Experimentally, the observed toroidal mode number is 2–3 for TFTR[2] and 2–10 in DIII-D.[3]

There already exists an extensive theoretical study[5–10] of the TAE mode for low ($n \simeq 1$) or moderate ($n \sim 2$–3) mode numbers. The high-n TAE mode was first formulated and studied by Cheng *et al.*[11] A detailed study was performed recently by Fu and Cheng,[12] based on an analytic approximation for a circular equilibrium. In this work, we concentrate on the numerical study of the high-n TAE mode for a finite β equilibrium with a general cross-sectional shape.

In a finite β plasma with a general cross-sectional shape, the Alfvén spectrum gap is affected by the equilibrium cross-sectional shape and the plasma β, in addition to the profiles in q and density. In Sec. II, we give a general formulation of the method for finding this spectrum gap. A numerical code based on CONT[5] was used to study the dependence of this gap on the plasma equilibrium properties. Two different approximations for determining this gap are then discussed. One of these, the slow sound approximation, which takes into account the lowest-order effects due to the sound wave coupling, has been found to give correctly the overall gap structure. A brief conclusion on the results of this section is then presented. In Sec. III, a general formulation[13] of the equations appropriate for determining the high-n TAE mode in the ideal magnetohydrodynamic (MHD) model is first discussed. These equations are shown to approach asymptotically the equations for determining the gap structure in Sec. II. In general, a fourth-order set of differential equations needs to be solved. For modes at the TAE frequency, the equations may be solved iteratively, taking higher-order corrections of the sound wave effects into account. A second-order set of equations may be obtained by retaining the equivalent lowest-order correction of the sound waves, as used in the slow sound approximation. It also asymptotically reproduces the correct overall gap structure. This equation is solved numerically by using the computer code MBC.[14] It is found that high shear moves the mode frequency from the bottom of the gap toward the top, as was first shown in Ref. 11. The finite β effect moves the frequency back toward the bottom, as was first shown in Ref. 12. In general, the mode is found in the ballooning mode stable region and is not found in the ballooning unstable region, but the two modes are not as mutually exclusive as found by Fu and Cheng.[12] A brief conclusion is then given at the end of the section. In Sec. IV, we give a brief summary of this paper.

II. THE SHEAR ALFVÉN SPECTRUM GAP

In this section, we study the gap structure of the shear Alfvén continuum. First, we generalize the equations for the shear Alfvén continuum[5] at finite n to obtain the equations that determine the continuum gap at high (∞) n. Simplifying physical assumptions of the equations and their consequences are then discussed. The Alfvén spectrum and the spectrum gap of these equations are then studied, and conclusions are drawn on the dependence of these gaps on the equilibrium properties of the plasma.

A. Equations for the shear Alfvén gap at high n

Shear Alfvén waves are magnetic perturbations of the plasma that propagate parallel to the magnetic field. In a uniform plasma, their frequency is given by the dispersion relation $\omega = |k_\parallel| v_A$. In the tokamak $k_\parallel \simeq (nq-m)/qR$, where n and m are the toroidal and poloidal mode numbers. Due to the continuous variation of q and v_A values across the flux surfaces, frequencies identified by each n

[a)]Permanent address: Princeton Plasma Physics Laboratory, Princeton, New Jersey 08543.

 0899-8213/92/113713-09$04.00

and m pair give rise to one continuum in the frequency spectrum of the Alfvén waves. On the flux surface of a tokamak, since v_A and other quantities vary on the flux surface, periodicity conditions couple the different m modes. The frequency of the Alfvén waves is then determined by an eigenvalue equation. Two branches, identified by (n,m) and (n,m') would have the same frequency at $q=(m+m')/2n$. The strong interaction of these two waves brought about by the coupling then gives rise to a gap in the spectrum,[15] similar to the spectral gap observed in the solid state. At the spectral gap boundary, the eigenfunction satisfies special periodic parity conditions. These conditions are the equations that determine the structure of these gaps.

The geodesic curvature on the flux surface couples the sound waves to the Alfvén waves. Sound waves satisfy the dispersion relation, $\omega=k_{\|}c_s$; and $c_s/v_A=\sqrt{\beta}$. A tokamak has $\beta<1$. At low frequency, an Alfvén wave with low $k_{\|}$ can be strongly affected by sound waves with higher $k_{\|}$. Results from the present work indicate that a new gap is created by this effect.

The equations for determining the Alfvén waves have been discussed by various authors. Here, we mainly follow the exposition given by Cheng and Chance,[5] except we point out the relationship between the Floquet theorem and the parity conditions for the eigenfunctions. We adopt the magnetic field representation

$$\mathbf{B}=\nabla\zeta\times\nabla\psi+q(\psi)\nabla\psi\times\nabla\theta,$$

with the Jacobian $J=(\nabla\psi\times\nabla\theta\cdot\nabla\zeta)^{-1}$. The MHD equations for determining the response of the plasma to a radial displacement are given by Eq. (8) of their paper,

$$E\begin{pmatrix}\xi_s\\ \nabla\cdot\boldsymbol{\xi}\end{pmatrix}=F\begin{pmatrix}P_1\\ \xi_\psi\end{pmatrix}, \tag{1}$$

where $\boldsymbol{\xi}$ is the plasma displacement $\xi_\psi=\boldsymbol{\xi}\cdot\nabla\psi$, $\xi_s=\boldsymbol{\xi}\cdot(\mathbf{B}\times\nabla\psi)/|\nabla\psi|^2$, and $P_1=p_1+\mathbf{b}\cdot\mathbf{B}$. The nontrivial solution of Eq. (1) on the flux surface, namely

$$E\begin{pmatrix}\xi_s\\ \nabla\cdot\boldsymbol{\xi}\end{pmatrix}=0, \tag{2}$$

determine the resonant Alfvén and sound waves on the flux surface. In (1) and (2), E is the matrix operator

$$\begin{aligned}
E_{11}&=\frac{\omega^2\rho|\nabla\psi|^2}{B^2}+(\mathbf{B}\cdot\nabla)\left(\frac{|\nabla\psi|^2}{B^2}(\mathbf{B}\cdot\nabla)\right),\\
E_{12}&=\gamma_s p\kappa_s,\\
E_{21}&=\kappa_s,\\
E_{22}&=\frac{\gamma_s p+B^2}{B^2}+\frac{\gamma_s p}{\omega^2\rho}(\mathbf{B}\cdot\nabla)\frac{1}{B^2}(\mathbf{B}\cdot\nabla),
\end{aligned} \tag{3}$$

where $\kappa_\psi=2\boldsymbol{\kappa}\cdot\nabla\psi$, $\kappa_s=2\boldsymbol{\kappa}\cdot[(\mathbf{B}\times\nabla\psi)/B^2]$, and $\boldsymbol{\kappa}=(\mathbf{B}/B)\cdot\nabla(\mathbf{B}/B)$ is the curvature. Since ζ is an ignorable coordinate for axisymmetric equilibria, the perturbed quantities may be written in the form

$$f(\theta,\zeta)=f_0(\theta)e^{-in\zeta}. \tag{4}$$

Thus

$$\mathbf{B}\cdot\nabla\xi=J^{-1}e^{inq}\frac{\partial}{\partial\theta}(\xi e^{-inq\theta}), \tag{5}$$

and Eq. (2) reduces to

$$\begin{aligned}
&\frac{\omega^2\rho|\nabla\psi|^2}{B^2}Y_1+\frac{1}{J}\frac{\partial}{\partial\theta}\left(\frac{|\nabla\psi|^2}{B^2J}\frac{\partial}{\partial\theta}Y_1\right)+\gamma_s p\kappa_s Y_2=0,\\
&\kappa_s Y_1+\left(\frac{\gamma_s p+B^2}{B^2}\right)Y_2+\frac{\gamma_s p}{\omega^2\rho J}\frac{\partial}{\partial\theta}\left(\frac{1}{B^2J}\frac{\partial}{\partial\theta}Y_2\right)=0,
\end{aligned} \tag{6}$$

where $Y_1(\theta)=\xi_s\exp[in(\zeta-q\theta)]$, $Y_2(\theta)=(\nabla\cdot\boldsymbol{\xi})\times\exp[in(\zeta-q\theta)]$. Because the coefficients of Eq. (6) are periodic in θ, then from the Floquet theorem, the solutions of Y_1 and Y_2 can be written as

$$Y_1(\theta)=\exp(i\alpha\theta)\tilde{Y}_1(\theta), \tag{7}$$

where $\tilde{Y}_1$ is periodic in θ with a period of 2π. According to the general theory of fourth-order differential equations with periodic coefficients, for each value of ω^2 there are four values of α. For the case of interest here where the two equations (6) are weakly coupled, the values of α come in pairs with opposite sign. Then, for each such pair, the sum

$$R=e^{2\pi i\alpha}+e^{-2\pi i\alpha},$$

is a real analytic function of ω^2. Further, this sum oscillates as a function of ω^2 between values less than -2 and larger than $+2$. The quantity α is real when $-2<R<+2$, and complex otherwise. Equation (6) has a periodic solution when $\alpha=l-nq$, where l is an integer, and this defines the resonant modes. It follows that at each magnetic surface there is a resonant mode for some value of n for each value of ω^2 for which R lies between -2 and $+2$. When R lies outside this range, there are no resonant modes, and thus there is a gap. The spectral gap boundaries occur at

$$\exp(i\alpha 2\pi)=\pm 1. \tag{8}$$

We classify the solution, satisfying the $+1$ relation in (8) as the even solution, that satisfying the -1 relation in (8) as the odd solution. As a matter of fact, since Eq. (6) actually consists of a pair of equations, we may have

$$\begin{aligned}
&Y_1(\theta+2\pi)=Q_1Y_1(\theta),\quad Q_1=\pm 1,\\
&Y_2(\theta+2\pi)=Q_2Y_2(\theta),\quad Q_2=\pm 1.
\end{aligned} \tag{9}$$

Equations (6), together with conditions (9), are the envelope equations. They are independent of n. In general, Q_1 is not required to be the same as Q_2. Thus, the envelope spectrum is split into four types: even–even, even–odd, odd–even, and odd–odd, depending on the values of Q_1 and Q_2. It is also interesting to note that the solution of condition (8) gives

$$2nq=(m+m')\begin{cases}m+m' \text{ even}, & Q=+1,\\ m+m' \text{ odd}, & Q=-1.\end{cases} \tag{10}$$

These are the locations at which the envelope frequency would be the same as the Alfvén frequency, and they determine the locations of the corresponding gaps for a given n.

We note that condition (9) does not destroy the hermiticity of Eq. (6). It still can be solved by developing a variational principle with the Lagrangian function given by

$$\mathcal{L}=\oint\left\{J\omega^2\rho\left(\frac{|\nabla\psi|^2}{B^2}|Y_1|^2+B^2|Z|^2\right)-\left[\frac{|\nabla\psi|^2}{JB^2}\left|\frac{\partial Y_1}{\partial\theta}\right|^2+\left(\frac{J\gamma_s PB^2}{\gamma_s P+B^2}\right)\left|\kappa_s Y_1-\frac{1}{J}\left(\frac{\partial Z}{\partial\theta}\right)\right|^2\right]\right\}d\theta, \tag{11}$$

where $Z=\gamma_s p[(\partial Y_2/\partial\theta)/(J\omega^2\rho B^2)]$. The variational equations of (11) may be written as a matrix equation for the Fourier amplitudes of Y_1 and Z. It is given by

$$Y_1=\sum_m a_m e^{im\theta}+b_m e^{i(m+1/2)\theta}, \tag{12}$$

where the a_m's are the coefficients of the even envelopes and b_m's are the coefficients of the odd envelopes. The matrix for determining the even–even envelopes may be written as

$$V\begin{pmatrix}a_m^A\\ a_m^s\end{pmatrix}=T\begin{pmatrix}a_m^A\\ a_m^s\end{pmatrix}, \tag{13}$$

where

$$V_{mm'}=\oint d\theta\begin{pmatrix}v_{11}&v_{12}\\ v_{21}&v_{22}\end{pmatrix}\exp[i(m-m')\theta],$$

$$v_{11}=(|\nabla\psi|^2/JB^2)mm'+J\gamma_s pB^2\kappa_s^2/(\gamma_s p+B^2),$$

$$v_{12}=-[\gamma_s pB^2\kappa_s/(\gamma_s p+B^2)]m',$$

$$v_{21}=-[\gamma_s pB^2\kappa_s/(\gamma_s p+B^2)]m,$$

$$v_{22}=[\gamma_s pB^2/J(\gamma_s p+B^2)]mm'.$$

The corresponding matrix for T is given by

$$t_{11}=J\omega^2\rho(|\nabla\psi|^2/B^2),$$
$$t_{12}=0,$$
$$t_{21}=0, \tag{14}$$
$$t_{22}=J\omega^2\rho B^2.$$

The corresponding matrix for the odd–odd envelope is obtained by the substitution $m\to m+\frac{1}{2}$ in (13). The Alfvén sound wave is normalized so that $T_A+T_s=1$, where $T_A=\Sigma_m t_{11}a_m^{A\,2}$ and $T_s=\Sigma_m t_{22}a_m^{s\,2}$. Due to the geodesic coupling effect on the flux surface given by v_{12} and v_{21} in (13), the polarization of the waves on the flux surface is not purely Alfvénic nor sonic. A specific solution is somewhat arbitrarily (see the discussion of Fig. 2) regarded as an Alfvén wave if $T_A>T_s$, and it is regarded as a sound wave if $T_s>T_A$.

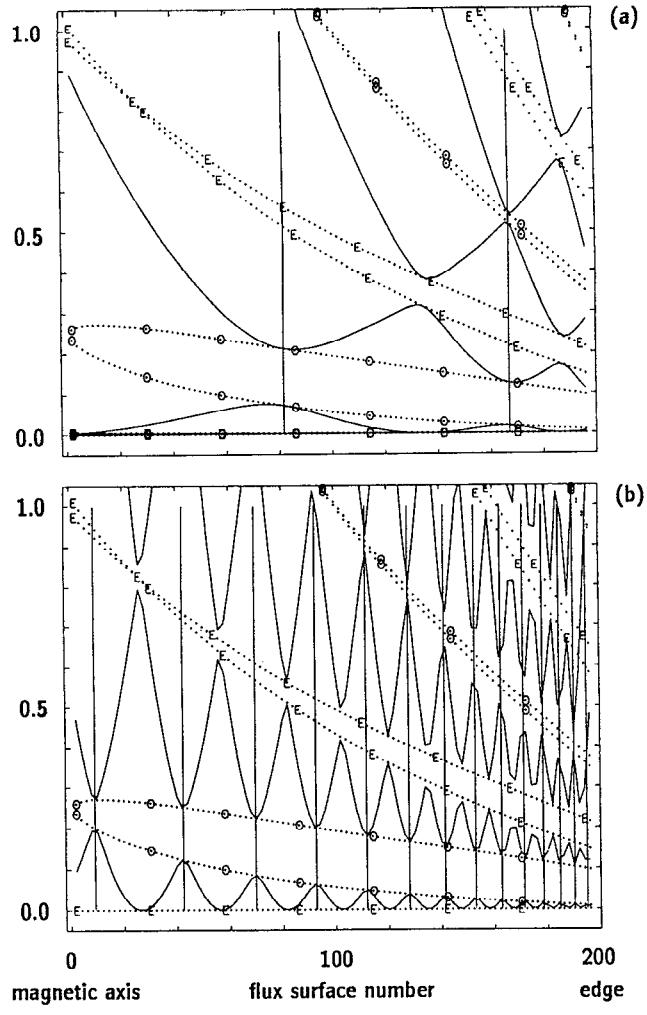

FIG. 1. Gap structure and Alfvén wave spectrum as a function of flux surface number with (a) toroidal mode number $n=1$ for a low (0%) β circular discharge in DIII-D. The magnetic axis is at surface number 0, the edge at surface number 197. The q value at the magnetic axis is 1.05 and it is 3.33 at the edge. The dotted curves are the envelopes. Curves marked with O are odd–odd envelopes and those marked with E are even–even envelopes. Vertical lines mark q values at which the Alfvén wave frequency matches the envelope frequency. (b) Gap structure and Alfvén wave spectrum for toroidal mode number $n=6$. As n number increases, the nature of the envelopes becomes prominent.

B. Numerical results of the Alfvén wave gap

The Alfvén wave spectrum code CONT has been modified to solve for the envelope equations given in (13). Shown in Fig. 1(a) is the gap structure together with the Alfvén wave spectrum for toroidal mode number $n=1$ for a low (0%) β circular discharge in DIII-D. The q value at the magnetic axis is 1.05, and it is 3.33 at the edge. The dotted curves are the envelopes. Those curves marked with O are the odd–odd envelopes and those marked with E are the even–even envelopes. The solid curves are the Alfvén

spectrum. The Alfvén wave spectrum is enclosed in between the odd–odd and even–even envelopes, whereas the Alfvén continuum gap lies between two odd–odd or even–even envelopes. Note that the lowest gap is an odd gap. The higher gaps alternate in odd and evenness. The vertical lines mark the q values at which the Alfvén wave frequency matches with the envelope given by Eq. (10) with $m'=m+1$. For the present equilibrium, the two q values are at $q=\frac{3}{2}$ and $\frac{5}{2}$. The reason for the existence of the first gap is mainly due to the $1/R$ dependence of the toroidal magnetic field on the flux surface. The first even gap above the odd gap exists due to higher-order coupling from toroidicity, including the elliptic deformation of the flux surface.[16,7] From Eq. (10) with $m'=m+2$, these envelopes have frequencies coincident with those of the Alfvén waves with $n=1$ at $q=2$ and 3 for this equilibrium. The next gap (an odd gap) is brought about by the triangular deformation of the flux surfaces and other higher-order coupling in a/R with the triangularity signature. They are characterized by Eq. (10) with $m'=m+3$. For $n=1$, the gap is thus at the value of $q=\frac{5}{2}$, etc. The envelope curves bound the Alfvén wave spectra and give the correct gap structure. This may be seen from Fig. 1(b), the topology of the frequency space plot for the same equilibria with $n=6$. It is clear that even at higher n, the Alfvén waves fill out the frequencies in between odd–odd and even–even envelopes while leaving gaps between the O–O and E–E envelopes.

At zero β, the sound wave frequencies are reduced to $\omega^2=0$. They are completely decoupled from the Alfvén waves. Therefore, all the modes shown at finite frequency in Fig. 1 are pure Alfvén waves. The picture is modified very drastically by increasing the pressure by a small (but finite) amount. Shown in Fig. 2(a) is the Alfvén sound wave frequency diagram for a DIII-D circular equilibrium with $\langle\beta\rangle=2\%$. The q value at the magnetic axis is 1.05, and it is 3.69 at the edge. Legends for the diagram are the same as those in Fig. 1(a). This indeed is a very complicated figure with a lot of information contained herein. By detailed examination, we may discern a group of waves with finite frequencies at the plasma center, and their frequencies reduce to zero at the plasma edge. These are the sound waves. They may be suppressed from the diagram by selectively plotting only modes with $T_A > T_s$. This is shown in Fig. 2(b). We note that the basic structure of Fig. 1(a) is then recovered. It is noticed that the first odd gap starts from the center at $\omega^2 \simeq 0.42\omega_A^2 > 0.25\omega_A^2$, and the first odd gap is much wider than that given in Fig. 1. Both of these effects have been predicted by Cheng.[1] It is also interesting to note that the envelopes that limit the Alfvén waves are then either the even–even or the odd–odd type. The even–odd and the odd–even types have been found to limit the sound waves. In Fig. 2, by comparing 2(b) with 2(a), it is seen that the sound waves do not observe the gap structure determined by the Alfvén waves. Thus, if a gap mode is located within the Alfvén gap, it could still be susceptible to damping through the excitation of these sound waves. It is also interesting to note that a zeroth gap appears before the first odd gap, i.e., Alfvén wave frequencies are confined

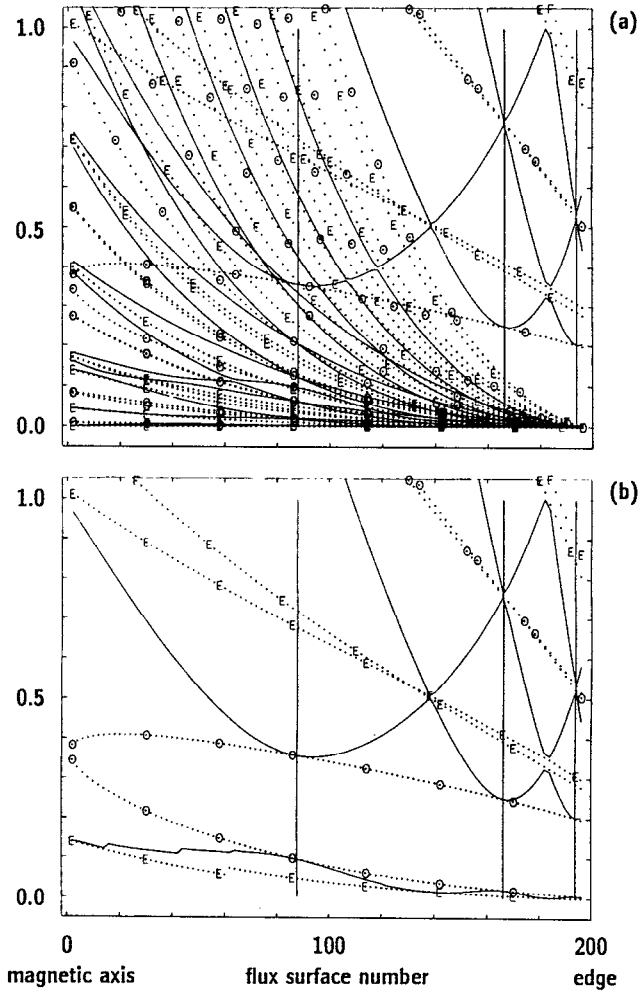

FIG. 2. Gap structure and Alfvén sound wave spectrum as a function of the flux surface number. The toroidal mode number is $n=1$ for a finite (2%) β circular equilibrium in DIII-D. (a) With the inclusion of sound waves. The magnetic axis is at surface number 0, the edge at surface number 197. The q value at the magnetic axis is 1.05 and it is 3.69 at the edge. Legends are the same as those in Fig. 1(a). A group of sound waves can be seen to have finite frequencies at the plasma center with frequencies reduced to zero at the edge. (b) Gap structure and Alfvén wave spectrum with sound waves suppressed. Finite β effects increase the frequency of the first odd gap and widens it. In addition, a zeroth even gap appears below the first odd gap.

to a band away from the $\omega^2=0$ axis. All waves with frequencies below the first even envelope show stronger characteristics of the sound wave rather than Alfvén waves. This system of sound waves interacts with itself, creates its own gaps, etc. It is an interesting subject by itself. However, we limit our study to only the Alfvén waves in the following and suppress all the sound waves in the figures.

To study the effect of ellipticity, we show in Fig. 3 the envelope and Alfvén wave frequency structure for a finite β (4.6%) DIII-D equilibrium with an elongation $\kappa=1.4$. It is seen that aside from the zeroth gap at very low frequency created by the finite β effect, and the first gap at $\omega^2 \sim 0.3$–$0.4\omega_A^2$, there appears a widened E–E gap emanating from the magnetic axis with $\omega^2 \simeq 1.0\omega_A^2$. The size of this gap is quite substantial due to the effect of ellipticity.[7,16]

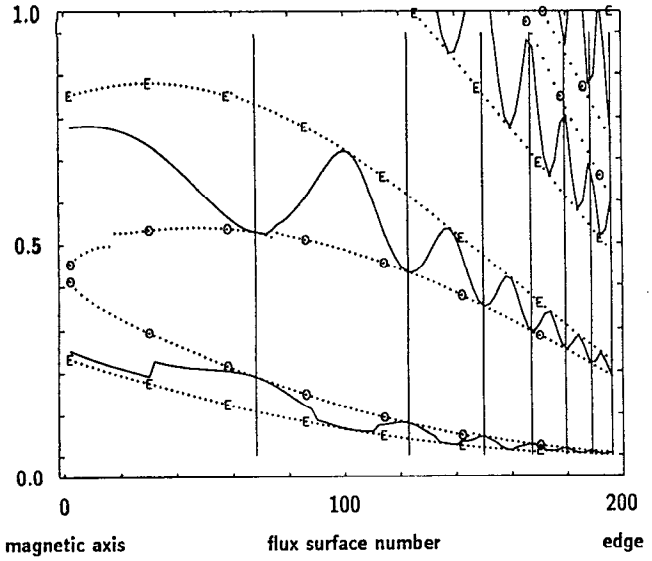

FIG. 3. Gap structure and Alfvén wave spectrum as a function of the flux surface number for a finite β (4.6%) DIII-D equilibrium with an elongation $\kappa=1.4$. The magnetic axis is at surface number 0, the edge is at surface number 197. A widened even gap emanates from the magnetic axis with $\omega^2 \simeq 1.0$.

We have also increased the triangularity of the plasma and verified that the next gap to appear is due to triangularity and can be made quite substantial in size by increasing the triangularity of the plasma cross section.

C. Approximate equations for the gap structure

1. div $\xi=0$

It is common in the study of Alfvén waves to adopt the approximation div $\xi=0$. In this case, $Y_2=0$ in Eq. (6). The Alfvén spectrum equation is then determined by

$$\frac{\omega^2\rho|\nabla\psi|^2}{B^2}Y_1+\frac{1}{J}\frac{\partial}{\partial\theta}\left(\frac{|\nabla\psi|^2}{B^2J}\frac{\partial}{\partial\theta}Y_1\right)=0. \tag{15}$$

The effect of this approximation on the structure of the Alfvén frequency spectrum is shown in Figs. 4(a) and 4(b). Figure 4(a) is the frequency and envelope structure for the $n=4$ mode for an elliptic DIII-D equilibrium; Fig. 4(b) is that obtained for Eq. (15). It is seen that imposing the div $\xi=0$ eliminated the zeroth gap and also lowered the frequency values of the structure throughout.

2. Slow sound approximation, $\gamma_s p/\omega^2\rho \ll 1$

In this approximation, (6) becomes

$$\frac{\omega^2\rho|\nabla\psi|^2}{B^2}Y_1+\frac{1}{J}\frac{\partial}{\partial\theta}\left(\frac{|\nabla\psi|^2}{B^2J}\frac{\partial}{\partial\theta}Y_1\right)-\frac{\gamma_s p\kappa_s^2B^2}{(\gamma_s p+B^2)}Y_1=0. \tag{16}$$

As shown in the next section, this is equivalent to the lowest consistent approximation with the inclusion of the effect of sound waves. The effect of this approximation on the structure of the Alfvén frequency spectrum is shown in Fig. 4(c). It is seen that this approximation captures the

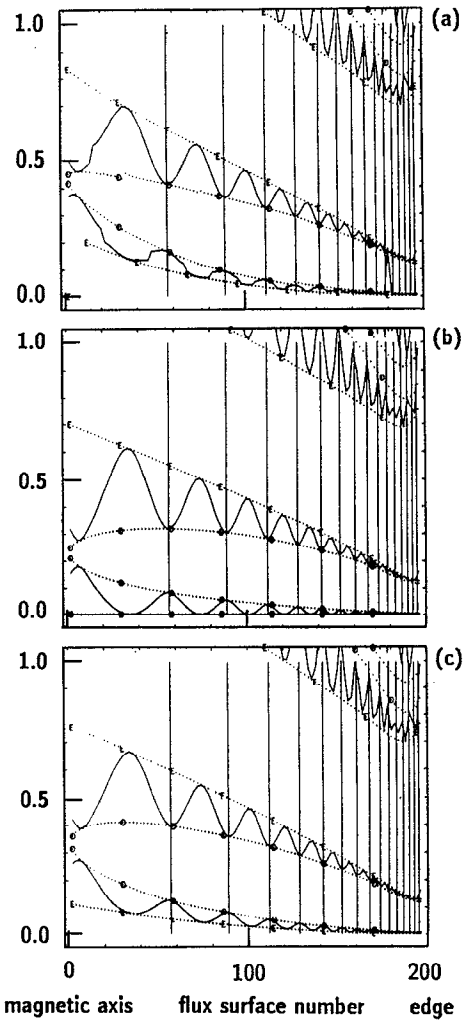

FIG. 4. Gap structure and envelope for $n=4$ for finite β elliptic DIII-D equilibrium as a function of the flux surface number. (a) With the inclusion of $\nabla\cdot\xi\neq0$ effects. The magnetic axis is at surface number 0, the edge at surface number 197. (b) The same as (a) with the $\nabla\cdot\xi=0$ approximation. It is seen that the zeroth gap is eliminated. Elimination of coupling to sound waves also shifts the whole diagram toward lower frequency values. (c) The same as (a) with the slow sound approximation. It is seen that the zeroth gap is reinstated. Restoration of the coupling to the sound waves also recovers most of the downshift in frequency observed in (b).

effect of the sound waves on Alfvén waves quite well and also reinstates the zeroth gap.

D. Summary

We summarize the results from the present section as follows.

(i) The envelope of the Alfvén frequency spectrum satisfies a gap equation given by Eq. (6) with conditions given by Eq. (9).

(ii) The frequency of the first gap is increased by the finite β effect. It is also widened by the finite β Shafranov shift.

(iii) Coupling of the Alfvén waves and the sound waves creates a zeroth gap at finite β.

(iv) Ellipticity creates a wide second gap.

(v) Triangularity widens the third gap.

(vi) In the up–down symmetric configurations studied, the gaps are always bounded by odd–odd or even–even envelopes.

III. THE HIGH-n GAP MODE

In this section, we study the MHD mode, which has its frequency in the gaps given by the envelopes determined in Sec. II. The high-n ideal shear Alfvén waves in tokamaks were first studied by Cheng *et al.*[11] Based on a force-free equilibrium, they have found that marginally stable toroidal shear Alfvén eigenmodes can exist inside the Alfvén spectrum gap. Finite β effect on these modes was subsequently studied by Fu and Cheng,[12] still neglecting the effect of sound waves. Based on a model equilibrium, they have found that the toroidicity-induced shear Alfvén eigenmodes are only found when the local pressure gradient is less than the critical pressure gradient value for ballooning instability. It is the purpose of this section to investigate the effect of shear and pressure gradients on this mode for a realistic equilibrium.

A. Equations for the high-n toroidicity-induced shear Alfvén eigenmode

The equations for high-n MHD modes at finite frequency have been given by Dewar and Glasser[13] to be

$$\frac{1}{J}\frac{\partial}{\partial\theta}\left(\frac{1}{J}\frac{k^2}{B^2}\frac{\partial\xi}{\partial\theta}\right)+\frac{2\boldsymbol{\kappa}\times\mathbf{B}\cdot\mathbf{k}}{B^2}\left[\frac{\gamma pB^2}{(B^2+\gamma p)}\left(\frac{1}{J}\frac{\partial\eta}{\partial\theta}-\frac{2\boldsymbol{\kappa}\times\mathbf{B}\cdot\mathbf{k}}{B^2}\xi\right)+p'\xi\right]+\frac{\omega^2\rho k^2}{B^2}\xi=0, \tag{17a}$$

$$\frac{1}{J}\frac{\partial}{\partial\theta}\left[\frac{\gamma pB^2}{(B^2+\gamma p)}\left(\frac{1}{J}\frac{\partial\eta}{\partial\theta}-\frac{2\boldsymbol{\kappa}\times\mathbf{B}\cdot\mathbf{k}}{B^2}\xi\right)\right]+\omega^2\rho B^2\eta=0. \tag{17b}$$

In (17), $\mathbf{k}=\nabla(\zeta-q\theta+q\theta_\kappa)$, and $\xi=\boldsymbol{\xi}\cdot\nabla\psi$, and $\eta=\boldsymbol{\xi}\cdot\mathbf{B}/B^2$. Here, θ_κ is a parameter. We first explore the structure of the set of Eqs. (17) and their relationship to Eq. (6). It is easy to verify that (17) is equivalent to the following set of Hamilton–Jacobi equations:

$$\frac{\partial\xi}{\partial\theta}=-P_\xi\frac{JB^2}{k^2}, \tag{18a}$$

$$\frac{\partial P_\xi}{\partial\theta}=-\frac{2\boldsymbol{\kappa}\cdot\mathbf{B}\times\mathbf{k}}{B^2}P_\eta J+\omega^2 J\frac{\rho k^2}{B^2}\xi+Jp'^2\frac{\boldsymbol{\kappa}\cdot\mathbf{B}\times\mathbf{k}}{B^2}\xi, \tag{18b}$$

$$\frac{\partial\eta}{\partial\theta}=-P_\eta\frac{(B^2+\gamma p)J}{\gamma pB^2}+\frac{2\boldsymbol{\kappa}\cdot\mathbf{B}\times\mathbf{k}}{B^2}\xi J, \tag{18c}$$

$$\frac{\partial P_\eta}{\partial\theta}=-\omega^2\rho B^2 J\eta, \tag{18d}$$

with the Hamiltonian

$$\mathcal{H}=-\frac{1}{2}P_\xi^2\frac{JB^2}{k^2}-\frac{1}{2}JP_\eta^2\frac{(B^2+\gamma p)}{\gamma pB^2}-\frac{1}{2}\omega^2\rho JB^2\eta^2-\frac{1}{2}\omega^2\frac{\rho k^2}{B^2}J\xi^2-\frac{1}{2}Jp'^2\frac{\boldsymbol{\kappa}\cdot\mathbf{B}\times\mathbf{k}}{B^2}\xi^2+P_\eta\frac{2\boldsymbol{\kappa}\cdot\mathbf{B}\times\mathbf{k}}{B^2}\xi J. \tag{19}$$

As $\theta\to\infty$, $\mathbf{k}\to-\theta q'\nabla\psi$, and the leading terms of (17) reduce to

$$\frac{1}{J}\frac{\partial}{\partial\theta}\left(\frac{|\nabla\psi|^2}{JB^2}\frac{\partial}{\partial\theta}\xi\right)-\frac{2\gamma_s P\kappa_s B^2}{(B^2+\gamma p)}\frac{1}{J}\frac{\partial\eta}{\partial\theta}-\frac{4\gamma_s P\kappa_s^2 B^2}{(B^2+\gamma p)}\xi+\omega^2\rho\frac{|\nabla\psi|^2}{B^2}\xi=0,$$
$$\frac{1}{J}\frac{\partial}{\partial\theta}\left(\frac{B^2\gamma p}{(B^2+\gamma p)}\frac{1}{J}\frac{\partial\eta}{\partial\theta}\right)+\frac{1}{J}\frac{\partial}{\partial\theta}\left(\frac{2\kappa_s B^2\gamma_s p}{(\gamma_s p+B^2)}\xi\right)+\omega^2\rho B^2\eta=0. \tag{20}$$

These are identical to the Euler–Lagrangian equations (6) of the Lagrangian of Eq. (11), with $\xi=y_1$, $\eta=Z$. We note the coupling of the sound waves (18c) and (18d) to the Alfvén waves (18a) and (18b) is through the P_η term in (18b). The full set of equations is fourth order in its highest derivative in θ. Here, instead of solving the complete set, we seek an approximation that retains the second-order nature of the Alfvén waves, as was done in Sec. II C 2.

Here (18c) and (18d) may be rewritten as

$$P_\eta=\gamma p\frac{B^2}{(B^2+\gamma p)}\left(\frac{2\boldsymbol{\kappa}\cdot\mathbf{B}\times\mathbf{k}}{B^2}\xi-\frac{1}{J}\frac{\partial\eta}{\partial\theta}\right),$$
$$\eta=\frac{1}{\omega^2\rho}\frac{1}{JB^2}\frac{\partial P_\eta}{\partial\theta}. \tag{21}$$

For a finite frequency Alfvén gap mode with $\rho\omega^2>\gamma p$, (21) may be solved in successive orders of $\gamma p/\rho\omega^2$ as

$$P_\eta^0=\gamma p\frac{B^2}{(B^2+\gamma p)}\frac{2\boldsymbol{\kappa}\cdot\mathbf{B}\times\mathbf{k}}{B^2}\xi,$$
$$\eta=0, \tag{22}$$

and the higher-order approximations

$$P_\eta^i=-\gamma p\frac{B^2}{(B^2+\gamma p)}\frac{1}{J}\frac{\partial\eta^i}{\partial\theta},$$
$$\eta^i=\frac{1}{\omega^2\rho}\frac{1}{JB^2}\frac{\partial P_\eta^{i-1}}{\partial\theta}. \tag{23}$$

Or equivalently,

$$\frac{1}{J}\frac{\partial}{\partial\theta}\left(\frac{k^2}{JB^2}\frac{\partial\xi}{\partial\theta}\right)+\frac{2\boldsymbol{\kappa}\times\mathbf{B}\cdot\mathbf{k}}{B^2}p'\xi+\frac{\omega^2\rho k^2}{B^2}\xi-\left(\frac{2\boldsymbol{\kappa}\times\mathbf{B}\cdot\mathbf{k}}{B^2}\right)^2\times\frac{\gamma pB^2}{(B^2+\gamma p)}\xi=\frac{2\boldsymbol{\kappa}\times\mathbf{B}\cdot\mathbf{k}}{B^2}\sum_{i=1}^{\infty}P_\eta^i, \tag{24}$$

where

$$P_\eta^j=-\frac{\gamma p}{\omega^2\rho}\frac{B^2}{(B^2+\gamma p)}\frac{1}{J}\frac{\partial}{\partial\theta}\left(\frac{1}{JB^2}\frac{\partial P_\eta^{j-1}}{\partial\theta}\right),$$

$$P_\eta^0=\gamma p[B^2/(B^2+\gamma p)][(2\kappa\times\mathrm{B}\cdot\mathbf{k})/B^2]\xi.$$

The terms on the right-hand side of (24) are the higher-order sound wave corrections. In the following study, we ignore the effect of these terms. The resultant equation is then

$$\frac{1}{J}\frac{\partial}{\partial\theta}\left(\frac{k^2}{JB^2}\frac{\partial\xi}{\partial\theta}\right)+\frac{2\kappa\times\mathrm{B}\cdot\mathbf{k}}{B^2}p'\xi-\left(\frac{2\kappa\times\mathrm{B}\cdot\mathbf{k}}{B^2}\right)^2\frac{\gamma pB^2}{(B^2+\gamma p)}\xi$$
$$+\frac{\omega^2\rho k^2}{B^2}\xi=0. \tag{25}$$

It is easy to verify that as $\theta\to\infty$, (25) reduces to (16). Its envelope equation has the correct frequency structure for waves at low frequency.

Formation of the TAE mode in the gap may be discerned by noting that as $\theta\to\infty$, the solution of (25) has to match to the eigensolutions of (16). Equation (16) is equivalent to the following pair of equations:

$$\frac{\partial\xi^\infty}{\partial\theta}=-P_\xi^\infty\frac{JB^2}{|\nabla\psi|^2},$$
$$\frac{\partial P^\infty}{\partial\theta}=\omega^2J\frac{\rho|\nabla\psi|^2}{B^2}\xi^\infty-\frac{\gamma_s p\kappa_s^2B^2}{(\gamma_s p+B^2)}\xi^\infty, \tag{26}$$

with periodic coefficients. This is a generalized Mathieu equation. Following the development of Eq. (7) and below, with $\lambda=i\alpha$, the two independent solutions are periodic functions multiplied by exponentials,

$$\xi^\infty=\xi_1^\infty(\theta)e^{\lambda_1\theta}+\xi_2^\infty e^{\lambda_2\theta}. \tag{27}$$

The advantage of the formulation in (26) is that a Wronskian form, using the two independent solutions,

$$W=\begin{pmatrix}\xi_1^\infty & \xi_2^\infty\\ P_1^\infty & P_2^\infty\end{pmatrix},$$

satisfies

$$\frac{\partial}{\partial\theta}(\mathrm{Det}\ W)=0.$$

To calculate the value of the two λ's, we integrate two solutions over a full period 2π, with the initial conditions

$$\xi_1^\infty(0)=1,\quad P_1^\infty(0)=0,$$

and

$$\xi_2^\infty(0)=0,\quad P_2^\infty(0)=1.$$

Thus, $\mathrm{Det}(W)=1$, for all θ, since the Wronskian is constant. We may now evaluate

$$W(2\pi)=\begin{pmatrix}\xi_1(2\pi) & \xi_2(2\pi)\\ P_1(2\pi) & P_2(2\pi)\end{pmatrix}.$$

The eigenvalues λ of $W(2\pi)$ determine the behavior of the solutions, and the eigenvalues are determined by $\mathrm{Trace}[W(2\pi)]$. Note the $\mathrm{Trace}[W(2\pi)]$ depends on ω^2, so

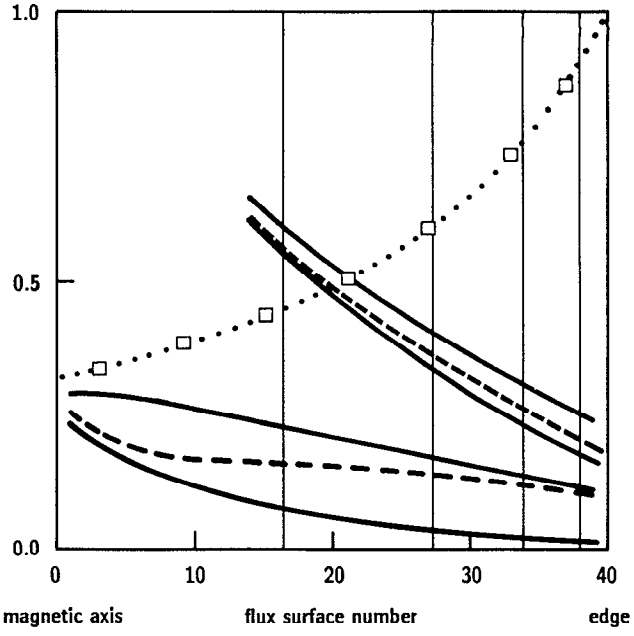

FIG. 5. Gap mode frequency as a function of flux surface number with $\theta_\kappa=0$ found for the DIII-D circle studied in Fig. 1. The magnetic axis is at flux surface number 0, the edge at surface number 40. A mode is found both in the first and second gaps. Solid curves show gap boundary, whereas dotted lines represent gap mode frequencies. The curve marked with □'s is the q value curve. It is 1.05 at the magnetic axis and 3.33 at the plasma edge. Vertical lines show q values of 1.5, 2.0, 2.5, and 3.0.

the eigenvalues of W depend on ω^2. For values of ω^2 for which $|\mathrm{Trace}(W)|<2$, the quantities λ are both pure imaginary, the frequency is in the Alfvén continuum. For values of ω^2 for which $|\mathrm{Trace}(W)|>2$, one of the λ is positive, it lies in the gap. Therefore, gap modes are the solution of (25) that are asymptotically matched to the damped solutions as $\theta\to\pm\infty$.

We have solved Eq. (25) numerically for exponentially damped solutions. They have been found to be in the gaps obtained by the method described in Sec. II. They also satisfy the criterion $|\mathrm{Trace}(W)|>2$. In general, it is found that $|\mathrm{Trace}(W)|<-2$ for solutions in the odd gaps and $|\mathrm{Trace}(W)|>2$ for solutions in the even gaps.

B. Numerical results of the Alfvén gap mode

The numerical equilibria studied for their gap structure have been analyzed to determine the dependence of the gap mode frequency on the equilibrium properties. Shown in Fig. 5 is the gap mode frequency with $\theta_\kappa=0$, which was found for the DIII-D circle studied in Fig. 1. A mode localized to $\theta\sim0$ is found both in the first and the second gap. The mode in the first gap has an even parity, i.e., $\xi(\theta)=\xi(-\theta)$, with a wavelength $\sim4\pi$ in θ; whereas, the mode in the second gap has an odd parity with a wavelength $\sim2\pi$ in θ. The dotted line marked by +'s is the curve for q. We note that for the mode in the first gap, its mode frequency near the magnetic axis lies toward the bottom of the gap due to the relative low shear near the magnetic axis. Toward the edge, where the magnetic shear

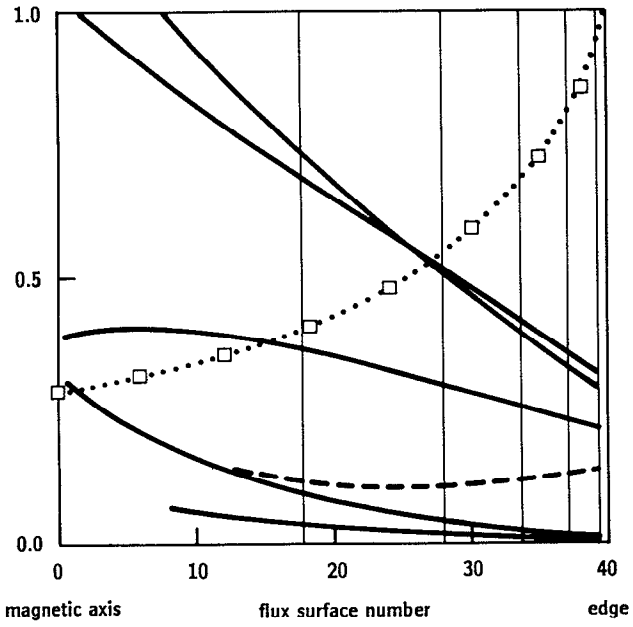

FIG. 6. Same as Fig. 5 for a 2% β circle in DIII-D. Increasing β moves the mode trajectory toward the bottom of the gap. Solid curves show gap boundary, whereas dotted lines represent gap mode frequencies. It is not found in the central portion of the plasma, nor is it found in the second gap. This configuration is stable to ballooning modes throughout the whole plasma cross section. The curve marked with □'s is the q value curve. It is 1.05 at the magnetic axis and 3.69 at the edge. Vertical lines show q values of 1.5, 2.0, 2.5, 3.0, and 3.5.

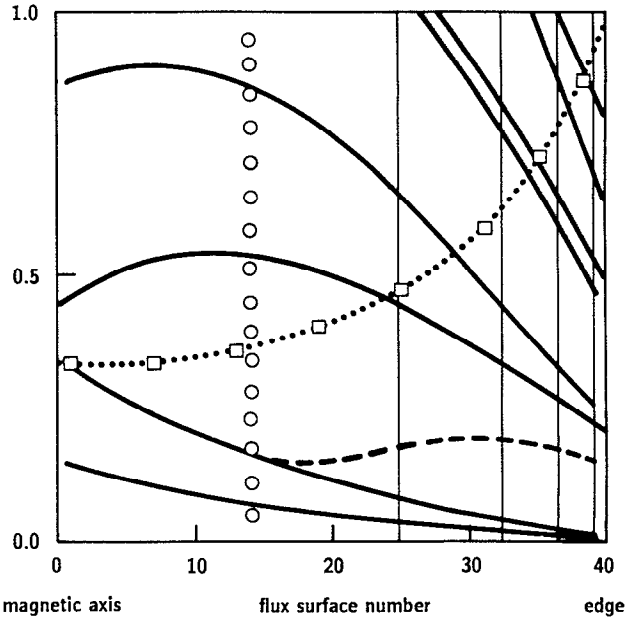

FIG. 7. Gap structure and mode frequency as a function of flux surface number with $\theta_\kappa=0$, for the ellipse studied in Fig. 3. The magnetic axis is at flux surface number 0, the edge at surface number 40. The mode is located outside the 35% flux surfaces. Localized ballooning mode analysis has shown that the plasma is ballooning unstable inside the 35% flux surface, marked with ○. The curve marked with □'s is the q value curve. It is 1.05 at the magnetic axis and 3.22 at the edge. Vertical lines show q values of 1.5, 2.0, 2.5, and 3.0.

is high, the frequency is located near the top of the gap, as has been predicted by the analytic theories.[11] In general, the effect of ellipticity and triangularity does not have a dramatic effect on the location of the mode in the gap. However, the finite β effect does. This is shown in Fig. 6 for the 2% β circle studied in Fig. 2. Increasing the β value to 2% moves the mode trajectory toward the bottom of the gap,[12] and it is not found in the central portion of the plasma. This configuration is stable to ballooning modes throughout the whole plasma cross section. In Fig. 7 we show the location of the mode frequency for the ellipse shown in Fig. 3. It is seen that the mode is located outside of the 35% flux surface location. The localized ballooning mode analysis has shown that the plasma is ballooning unstable inside the 35% flux surface. Some other experimental cases have also been analyzed. We have covered a range of equilibria with $\beta_N=[\beta(\%)a(\mathrm{m})B(\mathrm{T})]/[I(\mathrm{MA})]$ up to 3.5. In most of the cases analyzed, the TAE modes are found. They are located outside the ballooning mode unstable region. It is sometimes observed that the gap mode can exist within the ballooning unstable region. Therefore, contrary to the results obtained based on the analytic equilibrium model, the ballooning modes and high-n gap modes are not mutually exclusive. The effect of finite β is to push the mode location toward the bottom of the gap. When this effect is strong, the mode disappears.

C. Summary

We summarize the results from the present section as follows.

(i) At low shear, the mode is located at the bottom of the gap.

(ii) At high shear, the mode is located near the top.

(iii) Finite β effect moves the mode toward the bottom of the gap, until its frequency is moved outside of the gap and the mode disappears.

(iv) Even at high $\beta_N\approx 3.5$, the mode is still present in DIII-D geometry. In general, it is located outside of the ballooning mode unstable region, although the two modes are not strictly mutually exclusive.

IV. SUMMARY AND DISCUSSION

In this paper we have numerically investigated the structure of the shear Alfvén spectrum gap and the high-n gap mode in a finite β tokamak with a general cross section. Many of the conclusions obtained previously by various authors based on analytic equilibria are verified. New results, due to improved treatment of the coupling to the sound waves, are also obtained.

The shear Alfvén spectrum gap for a general equilibrium is studied in Sec. II. The general equations for determining the gap structure are given in Sec. II A. It is shown that these are the same equations for the Alfvén waves[5] with special boundary conditions imposed by the Floquet theorem and periodicity considerations. In Sec. II B, the dependence of the gap structure on the plasma equilibrium properties such as elongation, triangularity, and β are then studied. Finite β has been shown to greatly complicate the structure of the frequency diagram. With the introduction

of the oscillation energy norm with $T_A+T_s=1$ in (14), the waves are easily classified as having Alfvén (with $T_A>T_s$) or sound (with $T_s>T_A$) polarization. The structure of the resultant Alfvén wave diagram is then analyzed. The features in these diagrams can be understood as continuous transformation from that of a zero β circle. Finite β has been found to induce a zeroth gap below the toroidicity gap. It is due to the coupling to the sound waves. This zeroth gap is absent when the $\nabla\cdot\xi=0$ condition is imposed, but is reproduced when the slow sound approximation is adopted, as shown in (ii) of Sec. II C.

We studied in Sec. III the properties of the high-n gap modes. The equations for determining the high-n MHD modes[13] were first discussed in Sec. III A. It consists of a pair of second-order differential equations for the coupled Alfvén and sound waves on the flux surface. In the large θ limit, they also reduce to the equations for determining the gap structure. For TAE modes, a slow sound approximation may be used to reduce the coupled set to a second-order equation, which retains the correct gap structure shown in ii of Sec. II C. The solution of the high-n TAE mode with the slow sound wave approximation is shown in Sec. III B. It is found that at low shear the mode is located near the bottom of the gap. At high shear, the mode moves toward the top. Finite β effect moves the mode frequency toward the bottom of the gap again. Due to this effect, the high-n TAE mode is usually found in the region where the plasma is stable to ideal ballooning modes. They are usually not found in the region where ideal ballooning modes are unstable. However, there is no definite mutually exclusive relationship, as shown in the studies of Fu and Cheng.[12] The high-n TAE mode was also found in the second gap.[7]

Most of the previous studies[11,12] on the high-n TAE modes are based on using the compressionless ($\nabla\cdot\xi=0$) approximation. As shown in Sec. II C, this approximation ignores the effect of geodesic curvature on the Alfvén waves and gives a poor approximation to the gap structure. High-n TAE modes are the high-n MHD modes located in the gap. They are determined by equations asymptotically matched to the equations determining the envelopes. It is thus expected that $\nabla\cdot\xi=0$ is also a poor approximation for determining the frequency distribution of the high-n gap mode. One possible remedy is to solve the system of Eqs. (17a) and (17b) exactly, with the requirement $T_A>T_s$. The other possible remedy is to seek an improved approximation. In this work, we employed the slow sound approximation of $\gamma_s p/\rho\omega^2 \ll 1$. It is found that it gives a good approximation to the structure of the gaps and their frequencies. It also eliminates the sound waves yet retains their effect on the Alfvén waves. It is thus suggested to be a good approximation that could be used in further studies.

The excitation of these high-n MHD modes by resonant energetic particles has been the subject of several recent studies.[17,18] In general, due to the fact that the diamagnetic frequency of the energetic particles has to satisfy the criterion of $\omega_h^*/\omega > 1$, higher n or more localized TAE modes are expected to be more easily excited than lower n, except at extremely localized energetic particle pressure profiles. These high-n modes are also expected to more readily affect the transport of the energetic particles. With a given frequency, at high β it is expected that these frequencies could match with the local sound wave frequency at some hotter (inner) portion of the plasma or the local Alfvén frequency[19,20] at some outer portion of the plasma. These could provide damping mechanisms to the waves.

ACKNOWLEDGMENTS

The authors acknowledge useful discussions with Dr. L. Chen, Dr. H. L. Berk, Dr. W. W. Heidbrink, Dr. E. J. Strait, and Professor M. N. Rosenbluth. They would also like to acknowledge Dr. T. S. Taylor for comments on the manuscript.

This is a report of work sponsored by the U.S. Department of Energy under Contracts No. DE-AC03-89ER53277 and No. DE-AC02-76-CHO-3073.

[1] G. Y. Fu and J. W. Van Dam, Phys. Fluids B **1**, 1949 (1989).
[2] K. L. Wong, R. J. Fonck, S. F. Paul, D. R. Roberts, E. D. Fredrickson, R. Nazikian, H. K. Park, M. Bell, N. L. Bretz, R. Budny, S. Cohen, G. W. Hammett, F. C. Jobes, D. M. Meade, S. S. Medley, D. Mueller, Y. Nagayama, D. K. Owens, and E. J. Synakowski, Phys. Rev. Lett. **66**, 1874 (1991).
[3] W. W. Heidbrink, E. J. Strait, E. Doyle, G. Sager, and R. Snider, Nucl. Fusion **31**, 1635 (1991).
[4] C. Z. Cheng, Phys. Fluids B **3**, 2463 (1991).
[5] C. Z. Cheng and M. S. Chance, Phys. Fluids **29**, 3695 (1986).
[6] H. L. Berk, J. W. Van Dam, Z. Guo, and D. M. Lindberg, Phys. Fluids B **4**, 1806 (1992).
[7] R. Betti and J. P. Freidberg, Phys. Fluids B **3**, 1865 (1991).
[8] C. Z. Cheng, Phys. Fluids B **2**, 1427 (1990).
[9] J. W. Van Dam, G. Y. Fu, and C. Z. Cheng, Fusion Technol. **18**, 461 (1990).
[10] C. Z. Cheng, G. Y. Fu, and J. W. Van Dam, in *Theory of Fusion Plasmas*, edited by J. Vaclavik, F. Troyon, and E. Sindoni (Editrice Compositori, Bologna, 1989), p. 259.
[11] C. Z. Cheng, L. Chen, and M. S. Chance, Ann. Phys. **161**, 21 (1985).
[12] G. Y. Fu and C. Z. Cheng, Phys. Fluids B **2**, 985 (1990).
[13] R. L. Dewar and A. H. Glasser, Phys. Fluids **26**, 3038 (1983).
[14] R. W. Moore, R. R. Dominguez, and M. S. Chu, Nucl. Fusion **25**, 1575 (1985).
[15] C. E. Kieras and J. A. Tataronis, J. Plasma Phys. **28**, 395 (1982).
[16] M. S. Chance, J. M. Greene, R. C. Grimm, and J. L. Johnson, Nucl. Fusion **17**, 65 (1977); A. D. Turnbull, M. S. Chu, M. S. Chance, J. M. Greene, L. L. Lao, and E. J. Strait, Phys. Fluids B **4**, 3451 (1992).
[17] L. Chen, in Ref. 10, p. 327.
[18] L. Chen, R. B. White, G. Rewolt, P. L. Colestock, P. H. Rutherford, M. N. Bussac, Y. P. Chen, F. J. Ke, and S. T. Tsai, in *Plasma Physics and Controlled Nuclear Fusion Research*, Nice, France, 1988 (International Atomic Energy Agency, Vienna, Austria, 1989), Vol. II, p. 77.
[19] F. Zonca and L. Chen, Phys. Rev. Lett. **68**, 592 (1992).
[20] M. N. Rosenbluth, H. L. Berk, D. M. Lindberg, and J. W. Van Dam, Phys. Rev. Lett. **68**, 596 (1992).